"Hydrothermal wrapping" with poly(4-vinylpyridine) introduces functionality: pH-sensitive core-shell carbon nanomaterials

31st December 2012

Hydrothermal Wrapping Introduces Functionality: pH-Sensitive Core-Shell Carbon Materials Based on Poly-(4-Vinylpyridine) Wrapped Carbon Nanoparticles

Katherine Lawrence[a], Geoffrey W. Nelson[b], John S. Foord[b], Mónica Felipe-Sotelo[c], Nick D. M. Evans[c], John M. Mitchels[a], Tony D. James[a], Fengjie Xia[a,d], and Frank Marken[a*]

[a] *Department of Chemistry, University of Bath, Claverton Down, Bath BA2 7AY, UK*

[b] *Chemistry Research Laboratories, Oxford University, South Parks Road, Oxford OX1 3TA, UK*

[c] *Department of Chemistry, Loughborough University, Loughborough, Leicestershire LE11 3TU, UK*

[d] *State Key Laboratory of Advanced Technology for Materials Synthesis and Processing, Wuhan University of Technology, 430070, China*

To be submitted to Journal of Materials Chemistry

Proofs to F. Marken

F.Marken@bath.ac.uk

Abstract

Negatively charged carbon nanoparticles (Emperor 2000, Cabot Corp.) are “wrapped” in poly-(4-vinylpyridine) cationomer and hydrothermally converted into a pH-responsive core-shell nano-composite. With a “thin shell” this nano-material (ca. 20-40 nm diameter) is water-insoluble but readily dispersed into ethanol and deposited onto electrodes. Zeta-potential measurements suggest a PZC at ca. pH 4.5 with negative functional groups dominating in the more alkaline range and positive functional groups dominating in acid. XPS data suggest carboxylate and pyridinium-like functional groups. This is further confirmed in voltammetric measurements for adsorbed cations (methylene blue) and adsorbed anions (indigo carmine). The specific capacitance reaches a maximum of 13 Fg^{-1} at the PZC indicative of a “double layer compression” effect within the nanoparticle shell.

Keywords: carbon nanoparticle; functionalisation; hydrothermal synthesis; voltammetry; pH-response; polymer, sensor.

1. Introduction

Nanocarbon materials are useful in electrochemical systems, in particular in sensors [1] and as electrocatalyst supports [2]. “Pure” nanocarbon materials based on nanotubes [3], nanofibers [4], nano-onions [5], and graphenes [6] are often investigated and employed in the assembly of functional films. Nanoparticulate materials based on “carbon blacks” [7] have the disadvantage of a less well-defined chemical structure but the benefits of large scale accessibility, low cost, and a proven safety record.

Functionalised nanocarbon materials are readily obtained by covalent binding [8,9], physisorption [10], or the interaction of polymers with carbon surfaces [11]. Functionalised carbon blacks are used in industry (e.g. phenylsulphonate-functionalised carbon nanoparticles known as Emperor 2000, Cabot Corp.) and are attracting renewed attention for electrochemical systems [12,13]. We have recently demonstrated anthraquinone-functionalised carbon nanoparticles [14], dopylated carbon nanoparticles for gas sensing [15], and dioctylamine functionalised carbon nanoparticles as nano-supports for lipids [16].

Hydrothermal transformation of carbon-rich precursor materials such as glucose [17], starch [18], cellulose [19], or chitosan [20] is known to yield carbon products with relatively poor electrochemical properties [21] due to incomplete surface carbonisation in contact with the aqueous phase. However, partially carbonised materials can be useful in the surface

functionalisation of conducting substrates and “hydrothermal wrapping” was introduced as a simple method, for example ,for the synthesis of pH-responsive nano-carbon composites [22]. This method has also been used to modified carbon-palladium nano-composites for selective catalysis [23].

Here, the cationomer poly-(4-vinyl-pyridine) or P4VP is employed in the hydrothermal wrapping process. Negatively charged Emperor 2000 particles are initially wrapped with P4VP poly-cation in aqueous solution and then treated under hydrothermal conditions at 200 ^{o}C to give a novel core-shell wrapped nano-composite with interesting properties. The shell formed from poly-(4-vinylpyridine) introduces both anion-binding and cation-binding sites on the positive and negative sides of the PZC, respectively. Perhaps more surprisingly, a maximum specific capacitance of this core-shell material is observed at the PZC. The properties are discussed in terms of shell charging.

2. Experimental

2.1. Chemical Reagents

All reagents were used as supplied, without further purification: Emperor 2000 phenylsulphonate-functionalised carbon nanoparticles (8-18 nm average diameter, Cabot Corporation), poly-(4-vinylpyridine) – typical M_w 60,000 (Aldrich), acetic acid (Aldrich, 99.7 %, ACS reagent), absolute ethanol (Sigma-Aldrich), ortho-phosphoric acid (Fisher Scientific), sodium hydroxide (Aldrich, Sigma ultra, 98 %), indigo carmine, certified

(Aldrich), methylene blue, certified (Aldrich). Demineralised and filtered water was obtained from a Thermo Scientific water purification system (Barnstead Nanopure) with not less than 18.2 MΩ resistivity. Argon (Pureshield, BOC) was employed to de-aerate solutions prior to voltammetric studies.

2.2. Instrumentation

Zeta potential measurements were obtained with a ZetaMaster S (Malvern Instruments Ltd., UK) calibrated with zeta potential transfer standard (- 50 ± 5 mV, Malvern Instruments Ltd., UK). Data was recorded and analysed using ZetaMaster S standard software PCS v1.41. X-ray photoelectron spectroscopy (XPS) was carried out with an Al Kα x-ray anode of 1486.6 eV. All peaks were calibrated to 285 eV, *i.e.* the adventitious C1s peak. To obtain transmission electron microscopy (TEM) images, a JEM1200EXII (JEOL, Japan) was employed. Elemental analysis was performed by Medac Ltd. (Surrey, UK). Voltammetric studies were performed using a microAutolab III potentiostat system (EcoChemie, Netherlands) was employed with a Pt wire counter electrode and a KCl-saturated Calomel reference electrode (SCE, Radiometer, Copenhagen). A 3 mm diameter glassy carbon electrode (BAS) served as the basis for the working electrode. All experiments were performed at 22 ± 2 ^{o}C.

2.3. Procedure I: Hydrothermal Synthesis of “Thin Shell” and “Thick Shell” P4VP-Wrapped Carbon Nanoparticles

The nanocomposite materials were initially prepared based on a literature procedure [21]. In brief, 0.1 g P4VP was added to 18 mL 2% acetic acid and dissolved by ultrasonication. 0.24 g

Emperor 2000 carbon nanoparticles were then added and using ultrasonication for 1 h, a stable suspension was formed. The black suspension was transferred into a Teflon-lined 125 mL high pressure reaction vessel (Parr Instrument Company, US) and sealed. The vessel was placed into the oven at room temperature before being heated to 200 ^{o}C, it was maintained at this temperature for 12 h before cooling back to room temperature. The solid product was collected by Büchner filtration, washed copiously with water and ethanol before drying in an 80 ^{o}C oven for 1 h. This yielded a “thin” shell nanocomposite material. For a “thick” shell material, the procedure was repeated with half as much carbon, 0.12 g Emperor 2000.

2.4. Procedure II: Electrode Preparation

A suspension of core-shell nanoparticles was prepared (3 mg per 1 mL ethanol, sonicated). A carbon film was created by direct deposition of the ethanolic core-shell nanoparticle suspension (typically 15 µL) onto a glassy carbon electrode; following solvent evaporation a carbonaceous film could be seen. For voltammetric investigations with adsorbed dyes, the modified electrode was immersed into a buffered solution of either methylene blue or indigo carmine for five minutes to allow adsorption. The electrodes were then rinsed in fresh phosphate buffer solution and dried before being transferred directly into aqueous electrolyte solution for voltammetric measurements.

3. Results and Discussion

3.1. Characterisation of Thin Shell Core-Shell Nanoparticles

Initial electrochemical characterisation (vide infra) suggested that only “thin shell” materials are of interest due to “thick shell” materials being completely electrochemically inert. Therefore only “thin shell” material is characterised here. TEM imaging shows that the core-shell nanoparticles have a tendency to form aggregates but there are also a number of individual particles that can be observed (see Figure 1). From TEM images, it can be estimated that the polymer-carbon nano-composite particles have a diameter of approximately 20 – 40 nm (cf. 8 – 18 nm for Emperor 2000), irregular shape, and the edges become less well defined presumably due to the polymeric covering. By comparison to previous reports of Emperor 2000 TEM data [21] similarities can be observed and different types of carbon are not distinguishable.

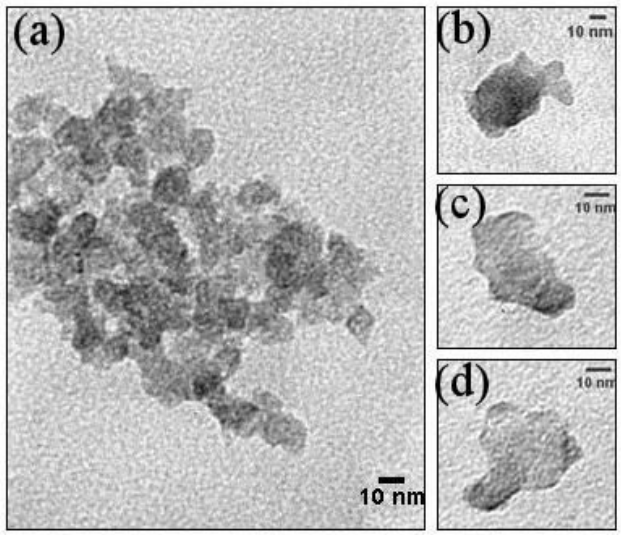

Figure 1. TEM images of hydrothermally P4VP-wrapped Emperor 2000 nanoparticle aggregates (a) and as individual particles (b)-(d); scale bar 10 nm.

Next, powder samples of P4VP-coated carbon nanoparticles were analysed by XPS (see Figure 2) to characterise the surface composition of the core-shell material. Two samples of the nanocomposite were investigated – one pre-washed with 0.1 M NaOH and another one pre-washed with 0.1 M HCl – in order to reveal surface functional groups.

The acid washed nanocomposite displayed a C1s peak that was assigned to two peaks associated with C-C/C-H and C-N at 285.0 and 286.4 eV, respectively (Figure 2a). The S2p signal at 168.8 eV is indicative of sulphonate [24] arising from the core of the material, Figure 2d, however the low S2p/C1s ratio implies that the sulphur signal is attenuated by the polymer shell. The N1s region can also be deconvoluted into two chemical environments. The peak with lower binding energy (399.3 eV) is assigned to the sp^2 hybridized nitrogen of the pyridine-like ring system. The peak with a slightly higher binding energy (401.1 eV) can be explained by the presence of protonated nitrogen in a pyridinium system [25]. Interaction of the pyridinium nitrogen (cation) with a chloride (anion) is likely and confirmed by the Cl2p spectrum (Figure 2e). The Cl2p peak appears to be associated with two forms of chloride, at 198.4 and 200.7 eV. These two peaks are not simply a doublet arising from spin-orbit coupling as the peak at lower binding energy would be of greater intensity [26,27].

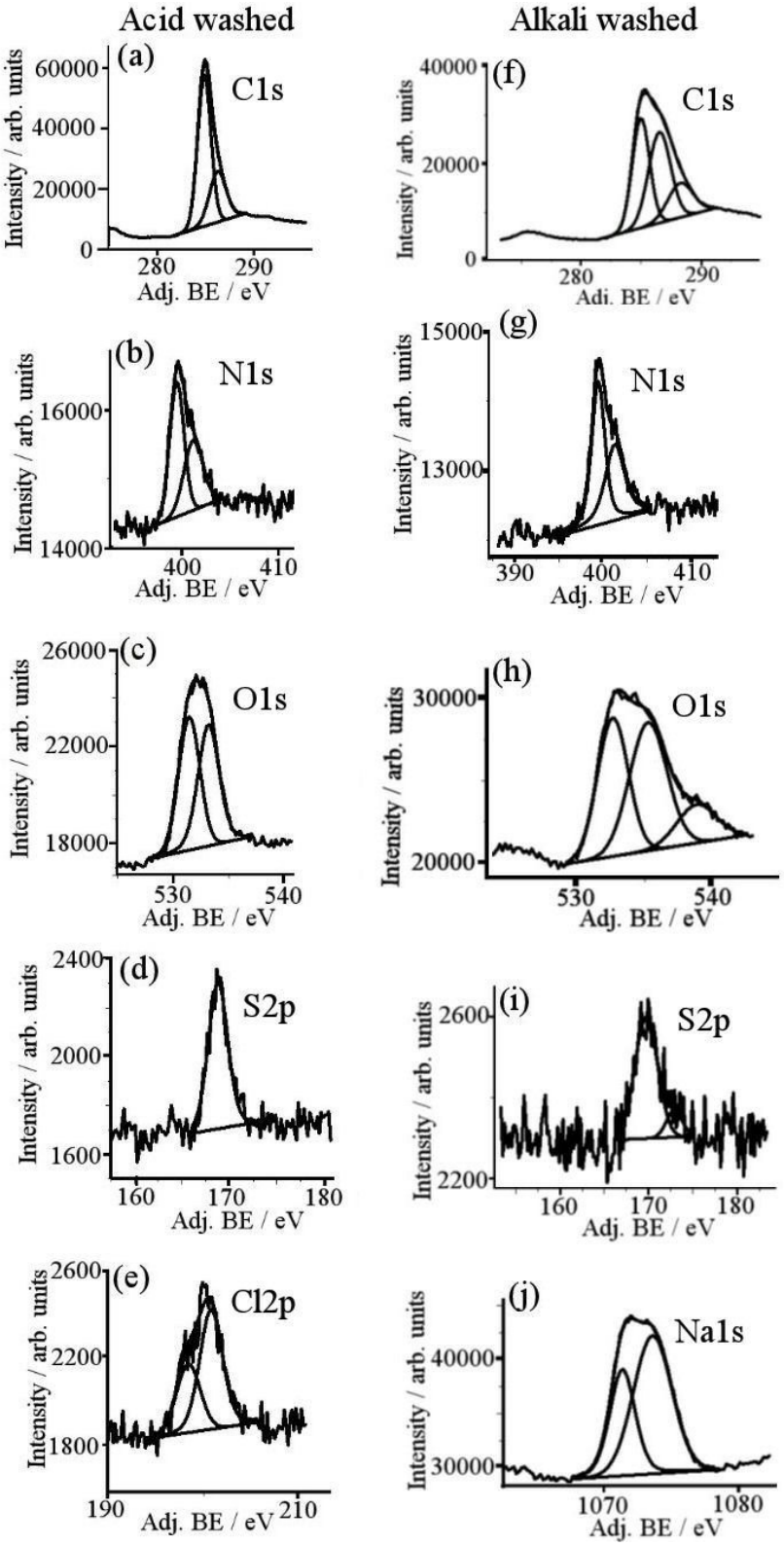

Figure 2. XPS data for core-shell nanoparticles (a) C1s (b) N1s (c) O1s (d) S2p (e) Cl2p pre-washed with 0.1 M HCl and (f) C1s (g) N1s (h) O1s (i) S2p (j) Na1s pre-washed with 0.1 M NaOH. Binding energies adjusted to C1s = 285 eV.

For the alkali-washed sample, the C1s and O1s spectra (see Figures 2f and 2h) can each be deconvoluted into three environments, in each case there is an additional signal at higher binding energy, with respect to the acid-washed sample. The higher binding energies are indicative of additional carbon and oxygen species being present in more electronegative environments, and suggest a greater carboxylate presence in the NaOH treated material than in the HCl treated shell. The N1s region shows again two signals, as was observed in the acid-washed equivalent (Figure 2g). This suggests that cation-bound nitrogen is still present (vide infra). The Na1s spectrum confirms the presence of sodium, which in NaOH would be seen at 1072.5 eV, whereas two peaks can be seen at -1.2 eV and + 1.1 eV, relative to the expected NaOH signal (Figure 2j). Sodium cations that are not involved or are only weakly involved in an ionic interaction tend to manifest at lower binding energies and could explain the peak seen at 1071.3 eV due to weak interactions with carboxylates. The peak at 1073.6 eV is indicative of Na^+ possibly interacting with nitrogen to produce the quaternary nitrogen species observed in the N1s spectrum [28]. Therefore, XPS shows two sodium interactions of which neither of which are due to residual NaOH, and are likely to be interactions with carboxylate oxygen and pyridine nitrogen.

XPS analysis confirms the core-shell structure of the nanocomposite with an Emperor 2000 core being coated by a film of carbonised P4VP. The core shows characteristic S2p peaks but these are low (as seen by the S2p/C1s ratio), demonstrating that the sulphur signal is well-attenuated by the polymer shell. In each case, the pyridine functionality is retained and demonstrated by ionic interactions. The N1s/C1s ratio is much higher for the NaOH washed sample (0.076 cf. 0.028), suggesting a greater amount of pyridine is present at the surface

when compared to the HCl washed material. The film thickness can be estimated using XPS employing Equation 1 [29]. Here, I is the intensity of the photoelectron signal of interest, I_{infinite} is the intensity expected for an infinitely thick film, t is the film thickness and λ is the photoelectron attenuation length.

$$\frac{I}{I_{\text{infinite}}} = \left(1 - e^{-\frac{t}{\lambda}}\right) \quad (1)$$

This calculation can be made by substituting the N1s/C1s ratio of the sample of interest in place of I, and I_{infinite} can be substituted with the N1s/C1s ratio of P4VP starting material. The photoelectron attenuation length is estimated following Equation 2, where B is a material parameter equal to 0.087 for organic layers and E_{kin} is the energy of the photoelectron of interest [30,31].

$$\lambda = B\sqrt{E_{kin}} \quad (2)$$

For an N1s photoelectron excited with Al Kα radiation through an organic overlayer, λ is approximately 2.8 nm. This approximate calculation gives an average shell thickness of 0.8 and 3.2 nm for acid and alkali washed core-shell carbon nanoparticles, respectively (with an error of ~15 %). The acid washed particles could have a decreased average shell thickness due to structural changes in the shell, but the assumption of the validity of I_{infinite} for both

cases is questionable here. Generally, a shell thickness of ca. 2-4 nm for the “thin shell” case is consistent with observations for chitosan-wrapped nanoparticles [22].

3.2. Electrochemical Characterisation I: Capacitive Responses

When the ethanolic suspension is drop-cast onto a glassy carbon electrode, a black water-insoluble film is produced. The modified electrode is then placed directly into an electrochemical cell with phosphate buffer and cyclic voltammetry experiments are performed. With an initial deposition amount of 60 µg of core-shell nanoparticles, a capacitance of ~1000 µF is observed (see Figure 3a).

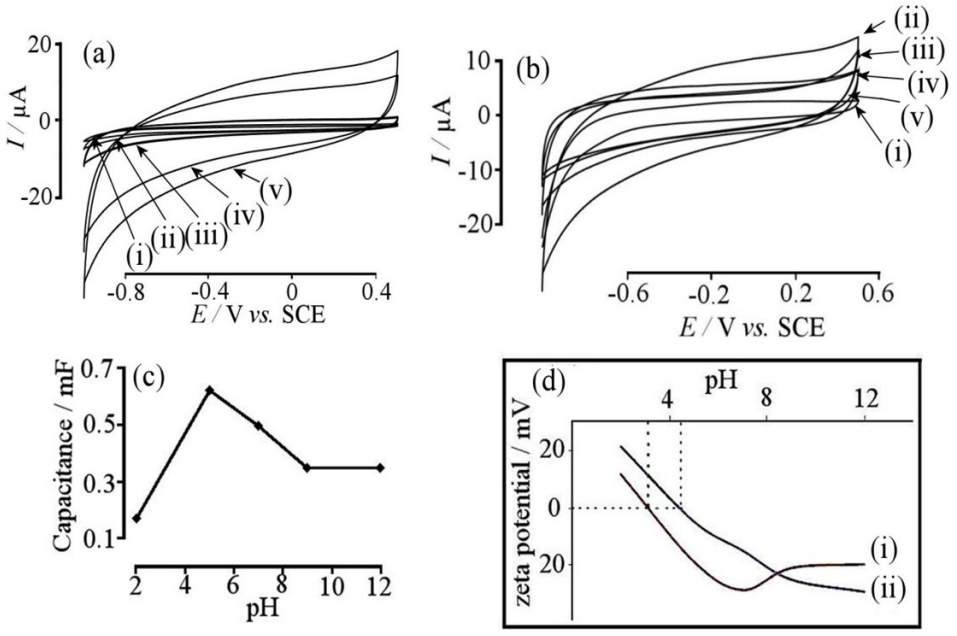

Figure 3. (a) Cyclic voltammograms (scan rate 10 mV s^{-1}) in 0.1 M phosphate buffer at pH 5 for (i) 0 µg (ii) 6 µg (iii) 15 µg (iv) 45 µg (v) 60 µg. (b) Cyclic voltammograms (scan rate 10 mV s^{-1}) with 45 µg deposit of CSNPs in 0.1 M phosphate buffer at pH (i) 2 (ii) 5 (iii) 7 (iv) 9 (v) 12. (c) Plot of capacitance as a function of pH. (d) Zeta potential measurements in 0.1 M phosphate buffer for (i) Emperor 2000 CNPs and (ii) for P4VP-wrapped carbon nanoparticles.

The capacitance of the core-shell nanoparticle film was investigated as a function of buffer pH (see Figure 3b and 3c). The lowest capacitance in the pH range 2 - 12 was observed when the pH of 0.1 M phosphate buffer was at pH 2. At pH 5 there was a large increase in the capacitance to ~0.65 F (= 13 Fg^{-1} specific capacitance). When the pH is increased further, the capacitance decreases again.

The zeta potential of the particles was measured and showed the PZC of the core-shell material to occur at approximately pH 4.5 (see Figure 3d). The similarity of point of maximum capacitance point and PZC suggests a possible link of both to the presence of ionic charges in the shell (vide infra). However, more complex scenarios involving resistivity as a function of pH cannot be ruled out.

3.3. Electrochemical Characterisation II: Faradaic Responses

To further investigate the surface charge of the core-shell material, the prepared electrodes were immersed into either a cationic or anionic redox-active dye and investigated as a function of concentration.

Methylene blue (used as a positively charged adsorption probe, see Figure 4) showed (at pH 7) a steady increase in current as the concentration of the dye solution was increased (see Figure 4a). The charge under the curve was extracted (see Figure 4b) and showed Langmuir-type behaviour with a maximum charge of approximately 9×10^{-4} C, which equates to 2.8 ×

10^{15} methylene blue molecules adsorbed into the core-shell nanoparticle film (assuming a two-electron process [32]). Interestingly, at lower concentration the oxidation, reduction and mid-point potentials all increased with increasing concentration of dye before levelling off at a constant value (see Figure 4c). The variation in mid-point potential is likely to be linked to a change in relative binding energy, i.e. at higher concentration the reduced form becomes more stable.

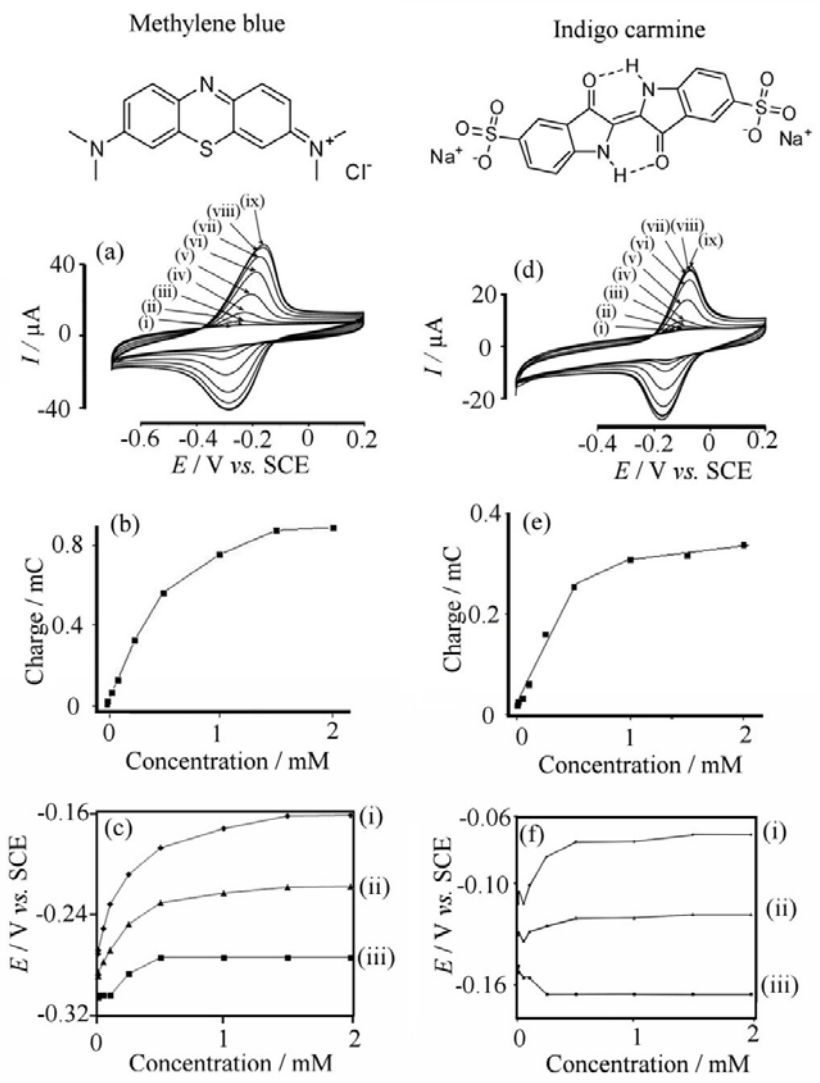

Figure 4. (a) and (d) Cyclic voltammograms (scan rate 10 mV s^{-1}) for 45 µg CSNP deposit dipped in dye solution for 5 minutes at concentrations of (i) 5 µM, (ii) 10 µM, (iii) 50 µM, (iv) 100 µM, (v) 250 µM, (vi) 500 µM, (vii) 1 mM, (viii) 1.5 mM and (ix) 2 mM in 0.1 M phosphate buffer solution (pH 7 for methylene blue and pH 3 for indigo carmine). (b) and (e) Plot of charge *vs*. concentration of dye. (c) and (f) Plot of peak potential *vs*. concentration of dye for (i) oxidation potential, (ii) mid-point potential and (iii) reduction potential.

Indigo carmine (used as a negatively charged adsorption probe, see Figure 4) showed (at pH 3) the same trend as methylene blue as the concentration of the adsorbed dye was increased (see Figure 4d). The charge under the curve once again led to a Langmuir-type curve that plateaued at approximately 3.3×10^{-4} C (see Figure 4e). This relates to a maximum number of adsorption sites on the CSNP film being approximately 4.1×10^{15} (assuming a two-electron process [33]). The oxidation and reduction peak-to-peak separation at low concentrations was approximately 75 mV which increased with increasing concentration to 95 mV. After the concentration reached 0.5 mM, the oxidation and reduction peak potential remained constant. The mid-point potential remained almost constant over the entire concentration range (see Figure 4f).

Zeta potential measurements showed that the PZC of the CSNPs occurs at ~pH 4.5. Therefore the effect dye adsorption at different pH values around pH 5 was investigated. Methylene blue, a cationic dye, showed the greatest Faradaic response at pH 7 (see Figure 5a). The Faradaic current progressively decreased in intensity as the pH became more acidic. This provides evidence that at higher pH values, the surface/shell of the nanoparticles has more anionic character. Interestingly, when the experiment was repeated for indigo carmine, an anionic dye, the opposite trend was observed. In this case, the greatest current was obtained at pH 3 (see Figure 5b). For both the anionic and cationic dye, the pH 5 signal showed a Faradaic current of a similar magnitude consistent with close to equal positive and negative charges at the core-shell nanoparticle surface.

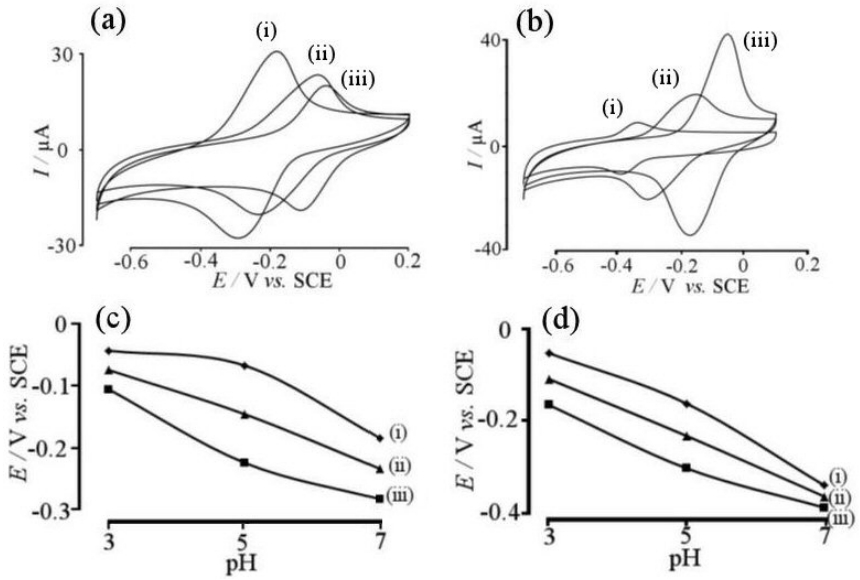

Figure 5. Cyclic voltammograms (scan rate 10 mV s^{-1}) for (a) methylene blue and (b) indigo carmine in 0.1 M phosphate buffer solution at pH (i) 7 (ii) 5 (iii) 3. Also shown are plots of (i) oxidation peak, (ii) mid-point, and (iii) reduction peak potentials for (c) methylene blue and (d) indigo carmine.

When looking at the oxidation peak, reduction peak, and mid-point potentials, there is a Nernstian shift of ~60 mV per pH unit. A decrease in peak-to-peak separation appears to occur at lower dye loading (see Figure 5c and 5d). Most importantly the presence of roughly equal amounts of positive and negative binding sites close to the PZC is implied for this type of core-shell nanoparticle material. In conjunction with the observation of the maximum capacitance at the PZC (vide supra) the following simplified model is proposed (see Figure 6). Immobilised cationic (pyridinium-like) and anionic (carboxylate-like) exist in the shell as a function of the solution pH. In the absence of additional electrolyte ions (the case of a dense shell) under acidic conditions the shell will be positively charged. Under alkaline conditions the shell will have more anion excess charges. At the PZC approximately equal amounts of positive and negative charges allow the extent of the double layer to decrease with a resulting increase in capacitance, i.e. the dielectric properties of the shell contribute to the observed capacitive current response.

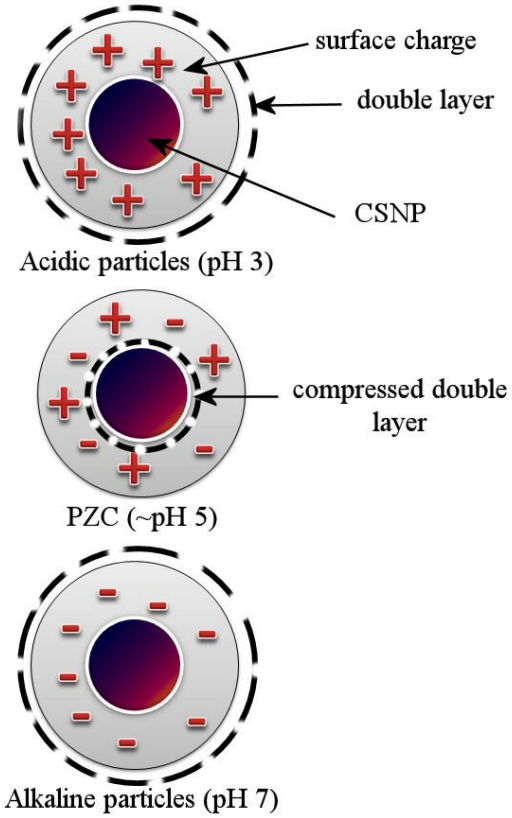

Figure 6. Schematic diagram of core-shell nanoparticles (CSNPs) at different pH to demonstrate the compression of the double layer at the PZC.

4. Conclusions

It has been shown that hydrothermal wrapping of negatively charged carbon nanoparticles with a poly-(4-vinyl-pyridine) precursor polymer results in the formation of a functional shell with strongly pH-dependent properties. The chemical structure of the carbonised material is not well-defined, however, the components pyridinium and carboxylate have been identified as positive and negative charge bearers. By adjusting the shell thickness, it was possible to produce a material with a maximum capacitive current (ca. 13 Fg^{-1} specific capacitance) at the

PZC and a model of “double layer compression” has been proposed. This type of core-shell nanomaterial could be useful for future sensing application for example when the proton-sensitivity is replaced by a more selective response to analytes such as heavy metals, pollutants, or trace bio-markers. A possible synthetic avenue will be the post-hydrothermal synthetic modification of the shell.

Acknowledgement

K.L. thanks the EPSRC for a DTA studentship to fund this research. This work was also supported by the CSC (China Scholarship Council, file number 2010695033) for F.X.

References

[1] H.L. Poh, M. Pumera, *Chem. Asian J.* 2012, **7**, 412.

[2] G.G. Wildgoose, C.E. Banks, R.G. Compton, *Small* 2006, **2**, 182.

[3] C. Gao, Z. Guo, J.H. Liu, X.J. Huang, *Nanoscale* 2012, **4**, 1948.

[4] A.V. Melechko, V.I. Merkulov, T.E. McKnight, M.A. Guillorn, K.L. Klein, D.H. Lowndes, M.L. Simpson, *J. Appl. Phys.* 2005, **97**, 041301.

[5] K.C. Hwang, *J. Phys. D-Appl. Phys*. 2010, **43**, 374001.

[6] Z.G. Zhu, L. Garcia-Gancedo, A.J. Flewitt, H.Q. Xie, F. Moussy, W.I. Milne, *Sensors* 2012, **12**, 5996.

[7] I.J. Sanders, T.L. Peeten, *Carbon Black: Production, Properties & Uses.* Nova Science Publishers Inc., London, 2011.

[8] F. Barriere, A.J. Downard, *J. Solid State Electrochem.* 2008, **12**, 1231.

[9] A.J. Downard, *Electroanalysis* 2000, **12**, 1085.

[10] T. Fujigaya, Y. Tanaka, N. Nakashima, *Electrochemistry* 2010, **78**, 2.

[11] U. Yogeswaran, S.M. Chen, *Anal. Lett.* 2008, **41**, 210.

[12] L. Vidal, A. Chisvert, A. Canals, E. Psillakis, A. Lapkin, F. Acosta, K.J. Edler, J.A. Holdaway, F. Marken, Anal. Chim. Acta 2008, 616, 28.

[13] T.W.B. Lo, L. Aldous, R.G. Compton, *Sens. Actuators B-Chem.* 2012, **162**, 361.

[14] J.D. Watkins, K. Lawrence, J.E. Taylor, T.D. James, S.D. Bull, F. Marken, *Electroanalysis* 2011, **23**, 1320.

[15] N. Bin Ibrahim, K. Lawrence, T.D. James, F.J. Xia, M. Pan, S.C. Mu, J.M. Mitchels, F. Marken, *Sens. Actuators B-Chem.* 2012, **161**, 184.

[16] K. Lawrence, J.D. Watkins, T.D. James, J.E. Taylor, S.D. Bull, G.W. Nelson, J.S. Foord, Y.T. Long, F. Marken, *Electroanalysis* 2012, **24**, 1003.

[17] T. Li, J.F. Shen, N. Li, M.X. Ye, *Mater. Lett.* 2012, **89**, 202.

[18] L.H. Yu, C. Falco, J. Weber, R.J. White, J.Y. Howe, M.M. Titirici, *Langmuir* 2012, **28**, 12373.

[19] M. Sevilla, A.B. Fuertes, *Carbon* 2009, **47**, 2281.

[20] Y.H. Yang, J.H. Cui, M.T. Zheng, C.F. Hu, S.Z. Tan, Y. Xiao, Q. Yang, Y.L. Liu, Chem. Commun. 2012, 48, 380.

[21] F.J. Xia, M. Pan, S.C. Mu, M.D. Jones, D. Wolverson, F. Marken, *Electroanalysis* 2012, **24**, 1703.

[22] F.J. Xia, M. Pan, S.C. Mu, Y.L. Xiong, K.J. Edler, I. Idini, M.D. Jones, S.C. Tsang, F. Marken, *Phys. Chem. Chem. Phys*. 2012, **14**, 15860.

[23] F.J. Xia, M. Pan, S.C. Mu, M.D. Jones, G. Kociok-Köhn, S.C. Tsang, F. Marken, *Electrochim. Acta*, 2013, in print.

[24] Wagner, C.D., et al., NIST X-ray Photoelectron Spectroscopy Database, N.I.o.S.a.T. (NIST), Editor. 2007, U.S. Secretary of Commerce, USA: Washington, USA

[25] D. Hulicova, J. Yamashita, Y. Soneda, H. Hatori, M. Kodama, *Chem. Mater*. 2005, **17**, 1241.

[26] X.D. Huang, S.H. Goh, *Polymer*, 2002. **43**, 1417.

[27] K.L. Tan, B.T.G. Tan, E.T. Kang, K.G. Neoh, *J. Chem. Phys.* 1991, **94**, 5382.

[28] S.N. Kumar, G. Bouyssoux, F. Gaillard, *Surf. Interface Anal*. 1990, **15**, 531.

[29] equation

[30] M. Textor, L. Ruiz, R. Hofer, A. Rossi, K. Feldman, G. Hahner, N.D. Spencer, *Langmuir* 2000, **16**, 3257.

[31] M.P. Seah, W.A. Dench, *Surf. Interface Anal.* 1979, **1**, 2.

[32] J.E. Halls, C.Y. Cummings, J. Ellis, L.L. Keenan, D.M. Jiang, A.D. Burrows, F. Marken, *Mol. Cryst. Liquid Cryst*. 2012, **554**, 12.

[33] M. Amiri, S. Shahrokhian, F. Marken, *Electroanalysis* 2007, **19**, 1032.